Support Information

Construction of excellent solid-state electrolyte by incorporating Li-IL into open-pore MOF/polymer-based materials

Zhi-Peng Ren[1], Bowei Cong[1], Feixue Xu[1], Shuyue Ouyang[2], Jia-Hui Zhao[2], Hao-Jie Yang[2], Shaohui Guo[1], Dongzheng Wu[3] & Xiaochuan Duan[1,3*], Xian-Ming Zhang[1,3*]

[1]Key Laboratory of Interface Science and Engineering in Advanced Materials Ministry of Education, Taiyuan University of Technology, Taiyuan 030024, China

[2]College of Chemical Engineering and Technology, Taiyuan University of Technology, Taiyuan 030024, China

[3]College of Chemistry, Taiyuan University of Technology, Taiyuan 030024, China

[*]Corresponding author emails:(zhangxianming@tyut.edu.cn,

duanxiaochuan@tyut.edu.cn)

1. Experimental Section

1.1 Experimental raw materials

Commercial polyacrylonitrile (PAN, M_W=150,000) was received from Sigma-Aldrich and was dried at 60℃ vacuum for 24 h before use. Copper nitrate ($Cu(NO_3)_2 \cdot 3H_2O$, 99.9%) was purchased from Aladdin. 1,3,5-Benzenetricarboxylic acid (H_3BTC, 99%) was purchased from Aladdin. Dimethyl sulfoxide (DMSO, 99%), N,N-dimethylformamide (DMF, 99.5%), and

methanol (MeOH, 99.5%) were purchased from Sinopharm Chemical ReagentCo., Ltd.

1.2 Preparation of HKUST-1/PAN via one-pot coaxial electrospinning strategy

The HKUST-1/PAN membrane was prepared using a one-pot coaxial electrospinning strategy modified from the one-pot electrospinning method. Firstly, 0.192g H_3BTC was dissolved into a mixture of 4mL DMF/DMSO (volume ratio 1:1), and at the same time of slow stirring, 0.4g PAN was dissolved into the solution, which was used as the coaxial electrospinning core layer electrospinning solution after magnetic stirring at 60℃ for 3h. Then, 0.204g $Cu(NO_3)_2 \cdot 3H_2O$ was dissolved into a mixture of 2mL DMF/DMSO (volume ratio 1:1), which was magnetically stirred for 30min and used as a coaxial electrospinning solution for the shell layer of electrospinning. The core electrospinning solution and shell electrospinning solution were respectively loaded into 5mL plastic syringes and coaxial electrospinning was carried out with a voltage of 19kV, the advancing speed of the core and shell solution was 0.4mL/h and 0.2mL/h respectively, the spinning time was 10h, and the distance between the tip and the collector was 15cm. The pristine composite fiber membranes of light blue color HKUST-1/PAN were prepared using the one-pot coaxial electrospinning strategy.

1.3 Activation of HKUST-1/PAN membrane

The light blue fiber membranes obtained by coaxial electrospinning was washed with methanol to remove the HKUST-1 precursor, and then soaked in methanol solution for 12h, and the methanol solution was replaced every 2h to fully remove the residual object in the MOF channel, and finally vacuumed at 100℃ for 5h. Purple HKUST-1/PAN composite fiber membrane with MOF channels open was obtained.

1.4 Preparation of partially activated HKUST-1/PAN

Similar to the preparation of HKUST-1/PAN via one-pot coaxial electrospinning strategy, but the shell layer and core layer polymer should be replaced respectively. The 4mL DMF/DMSO (1:1) solution of 0.408g $Cu(NO_3)_2 \cdot 3H_2O$ and 0.4g PAN was the core layer electrospinning solution. The 2mL DMF/DMSO (1:1) solution of 0.096g H_3BTC and 0.2g PAN was the outer shell electrospinning solution. Core-shell pushing velocity was 0.4mL/h and 0.2mL/h, respectively.

1.5 Preparation of Li-IL@HKUST-1/PAN CSE

Firstly the activated HKUST-1/PAN composite membrane was stamped into 16 mm discs. Then lithium bis(trifluoromethanesulfonyl)imide (LiTFSI) was dissolved in the ionic liquid 1-ethyl-3-methylimidazolium bis(trifluoro methane sulfonyl)imide ($[EMIM^+]$ $[TFSI^-]$) mixed as Li-IL ($[EMIM_{0.8}\ Li_{0.2}^+]$ $[TFSI^-]$) in a molar ratio of 2:8. Finally, the activated HKUST-1/PAN discs were immersed in Li-IL, and then vacuum dried at 100°C to obtain dark blue Li-IL@HKUST-1/PAN composite solid electrolyte. All the above operations were carried out in an argon atmosphere glove box (O_2 and $H_2O \leq 0.01$ ppm).

2. Characterization Section

2.1 Characterization Methods

The phase composition of the material was characterized by X-ray diffractometer (XRD, Rigaku SmartLab SE) at a test Angle of 5 to 50° and a scanning speed of 5°/min. The morphology of the materials was characterized by electron microscopy (SEM, JSM-7900F). The pore structure of the material was simulated by micropore absorption and desorption using a specific surface

analyzer (BET, Autosorb IQ). The thermal stability of the materials was characterized by thermogravimetric analyser (TGA, Rigaku STA8122) in an air atmosphere, tested at temperatures ranging from 25 to 800°C, with a ramp rate of 10°C/min. The chemical bonding and structural changes of the materials were tested and analysed by Fourier Transform Infrared Spectroscopy (FT-IR, BRUKER INVENIO S) at wavelengths ranging from 400 to 4000 cm^{-1}.

2.2 Electrochemical measurements

The CR2032 button cell was assembled for electrochemical performance testing in an argon atmosphere glove box (O_2 and $H_2O \leq 0.01$ ppm). AC impedance spectroscopy (EIS) and linear sweep voltammetry (LSV) tests were carried out with an electrochemical workstation (PARSTAT MC) , in which the frequency range of the EIS test was 0.01~10^5 Hz with an amplitude of 5 mV, and the LSV test voltage was from the open-circuit voltage to 7 V, with a sweep rate of 1 mV s^{-1}. The lithium-ion transference number was examined by assembling Li/CPE/Li symmetrical cells on the basis of

$$t_{Li+} = \frac{I_s\ (\Delta V - I_0 R_0)}{I_0\ (\Delta V - I_s R_s)}$$

where t_{Li+} presents the lithium ion transference number, ΔV is the applied DC polarization voltage of 10 mV, I_0 and I_s refer to initial and steady current, and R_0 and R_s indicate the resistance before and after polarization.

The weighed 12 mm $LiFePO_4$ positive electrode disc, 16 mm solid electrolyte, and 15.6 mm lithium metal negative electrode were taken and assembled and encapsulated sequentially Constant-current charge/discharge tests, and cycling performance tests were carried out with a LAND CT2001A with constant current density charge/discharge test: set the current according to

the demanded current density, and charge/discharge repeatedly for 30min each time; cycle performance test: charge and then discharge, with a charge/discharge voltage interval of 2.5~4.2V, and the first two cycles are activated with a multiplication rate of 0.2C (1C=170mAh/g).

2.3 Supplementary Tables and Figures

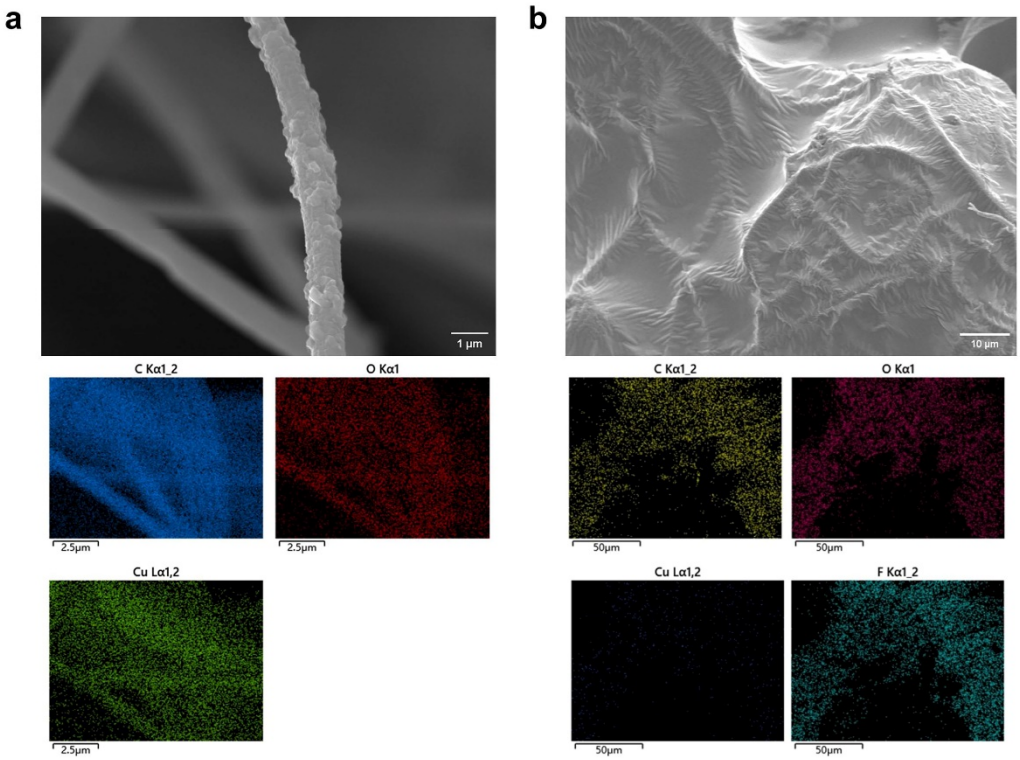

Fig. S1 SEM and the corresponding EDS mapping images (a) HKUST-1/PAN, (b) Li-IL@HKUST-1/PAN

Fig. S1 displays the SEM and the corresponding EDS mapping images schematically before and after loading of Li-IL on HKUST-1/PAN. It can be clearly seen that Li-IL is successfully encapsulated in MOF and uniformly distributed on the fiber surface.

Table S1 Ionic conductivity, activation energy and lithium-ion mobility of different SSEs

SSEs	Ionic conductivity (S cm^{-1})	Activation energy (eV)	Lithium-ion mobility	Ref.
P(PDEM-D4)-CSE	1.68×10^{-4} at 60°C	—	0.53	[1]
PEO-LLZTO	2.1×10^{-4} at 30°C	0.29	0.46	[2]
SCE	1.6×10^{-4} at 30°C	—	0.47	[3]
SSZ-13@PEO	1.91×10^{-3} at 60°C	—	0.5	[4]
M-S-PEGDA	2.26×10^{-3} at 30°C	—	0.44	[5]
M-UiO-66-NH-PEGDA	4.31×10^{-5} at 30°C	—	—	[6]
HSPE	9.83×10^{-4} at 25°C	0.26	0.68	[7]
IL@UiO-66	2.06×10^{-4} at 30°C	0.35	0.49	[8]
Li-IL@MOF-LLZO	1.0×10^{-4} at 30°C	—	0.18	[9]
Li-IL@MOF-525	3.0×10^{-4} at 25°C	—	0.36	[10]
Li-IL@HKUST-1	1.2×10^{-4} at 30°C	0.26	0.13	[11]
HKUST-1@Li-IL	0.68×10^{-4} at 25°C	0.34	0.46	[12]
Li-IL@HKUST-1/PAN	2.4×10^{-3} at 25°C	0.21	0.698	This work

The ionic conductivities, t_{Li+} and Ea values for this Li-IL@HKUST-1/PAN electrolyte are compared to those reported for solid electrolytes and shown in **Table S1**. These include the polymeric SSE P(PDEM-D4)-CSE (1.68×10^{-4} S cm^{-1}, 0.53 at 60°C)[1], and the ceramic SSEs PEO-LLZTO (2.1×10^{-4} S cm^{-1}, 0.46 at 30°C)[2], SCE (1.6×10^{-4} S cm^{-1}, 0.47 at 30°C)[3], and the MOF-based polymeric SSEs SSZ-13@PEO (1.91×10^{-3} S cm^{-1}, 0.5 at 60°C)[4], M-S-PEGDA (2.26×10^{-3} S cm^{-1}, 0.44 at 30°C)[5], HSPE (9.83×10^{-4} S cm^{-1}, 0.68 at 60°C)[7], and IL-loading MOF-based SSEs IL@UiO-66 (2.06×10^{-4} S cm^{-1}, 0.49 at 60°C)[8], Li-IL@MOF-LLZO (1.0×10^{-4} S cm^{-1}, 0.18 at 60°C)[9], Li-IL@MOF-525 (3.0×10^{-4} S cm^{-1}, 0.36 at 60°C)[10], HKUST-1@Li-IL (0.68×10^{-4} S cm^{-1},

0.46 at 60°C)[11]. Compared with these reported solid electrolytes, our Li-IL@HKUST-1/PAN CSE have excellent ionic conductivities (2.4×10^{-3} S cm^{-1}), high lithium-ion mobility (0.698) and low activation energy (0.21eV) at room temperatures.

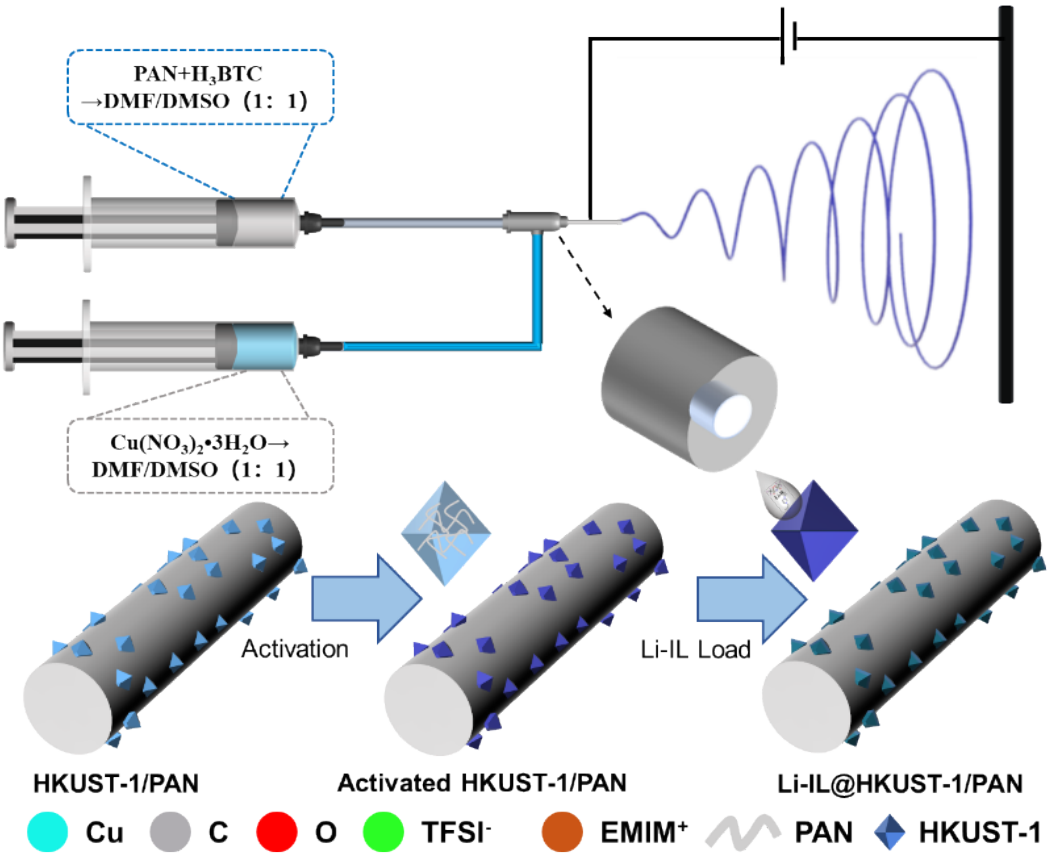

Fig. S2 Schematic of preparing Li-IL@HKUST-1/PAN SSE by one-pot coaxial electrospinning

Fig. S2 displays the schematic of preparing Li-IL@HKUST-1/PAN SSE by one-pot coaxial electrospinning.

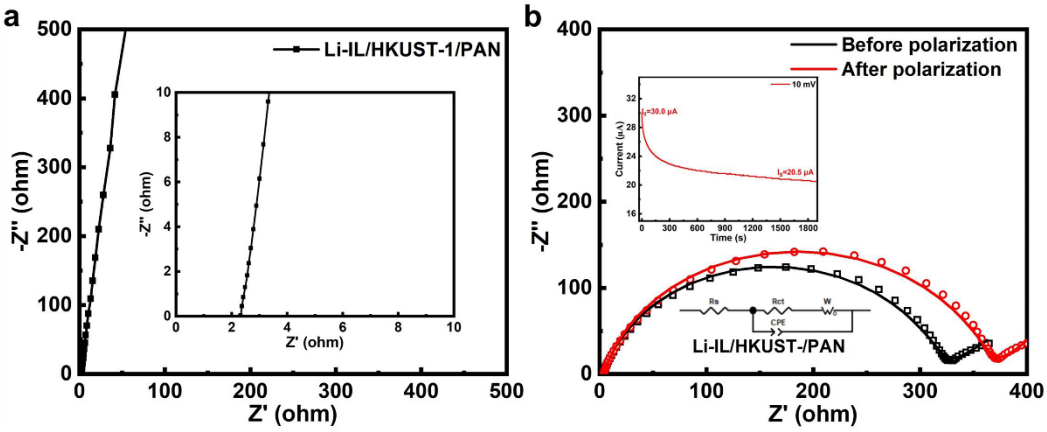

Fig. S3 Properties of Li-IL/HKUST-1/PAN: (a) AC impedance mapping of steel-sheet (ss) symmetric cells, (b) AC impedance mapping before and after constant voltage polarization of CSE (internal constant current polarization curve and equivalent circuit diagram)

Fig. S 3a displays the EIS pattern of a CSE-assembled steel-sheet (ss) symmetric cell. The cell has a thickness of 40 μm, an intrinsic impedance of 2.375 Ω, and a room temperature ionic conductivity of 8.32×10^{-4} S cm^{-1}. **Fig. S 3b** illustrates the impedance changes before and after constant potential polarization of CSE-assembled lithium symmetric batteries. The internal lithium ion mobility number of CSE is 0.17.

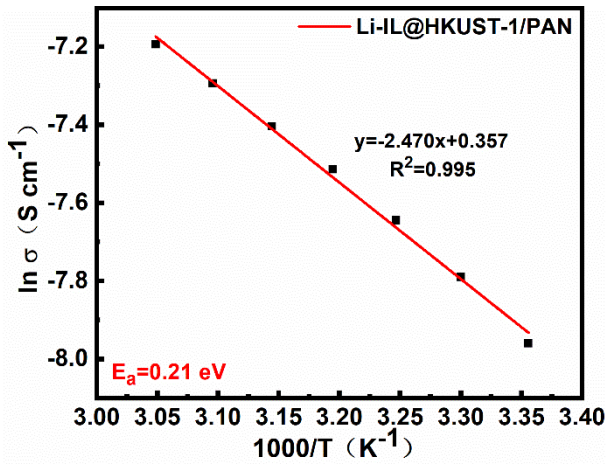

Fig. S4 The Arrhenius curve of Li-IL@HKUST-1/PAN CSE from 25°C to 55°C.

Fig. S4 displays the Arrhenius curve of CSE from 25°C to 55°C. The ionic conductivity of the CSE increases with temperature. The fitting of the curve yields an activation energy of 0.21 eV, indicating that Li^+ conduction is dependent on the pore and electrostatic interactions of MOF and Li-IL. This conduction is not limited by the slow relaxation motion of the polymer, which is consistent with the high room temperature ionic conductivity of CSE.

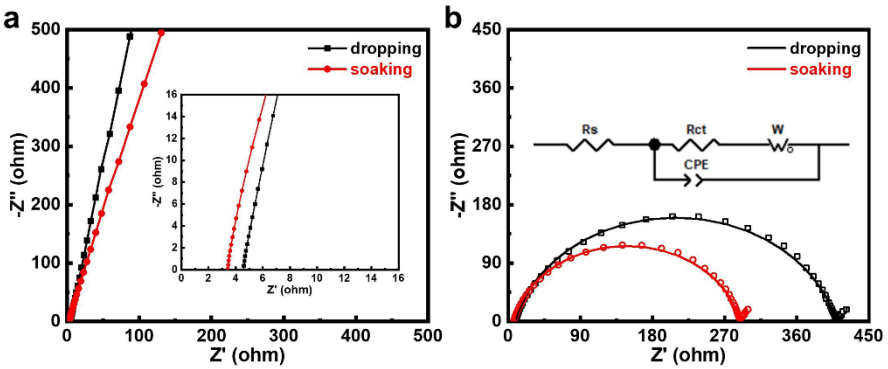

Fig. S5 (a) The ionic conductivity and (b) interfacial impedance of CSE after dropping or soaking Li-IL@HKUST-1/PAN SSE

We loaded Li-IL with HKUST-1/PAN in two different ways: dropping and soaking, where dropping was more favourable for improving the interfacial conductance and soaking was more favourable for improving the bulk conductance. **Fig. S5** displays the room temperature ionic conductivity and interfacial impedance of the CSE obtained from the two preparations clearly indicate that the electrochemical performance of the CSE after soaking (1.08×10^{-3} S cm^{-1}, 281.6 Ω) to improve the body conduction is superior to that of the CSE after dropping (8.64×10^{-4} S cm^{-1}, 399.2 Ω) to improve the interfacial conduction. This further demonstrates that loading Li-IL inside MOF to improve the bulk conduction of Li^+ can lead to the electrochemical performance of Li-IL@HKUST-1/PAN exceeding that of conventional Li-IL/HKUST-1/PAN.

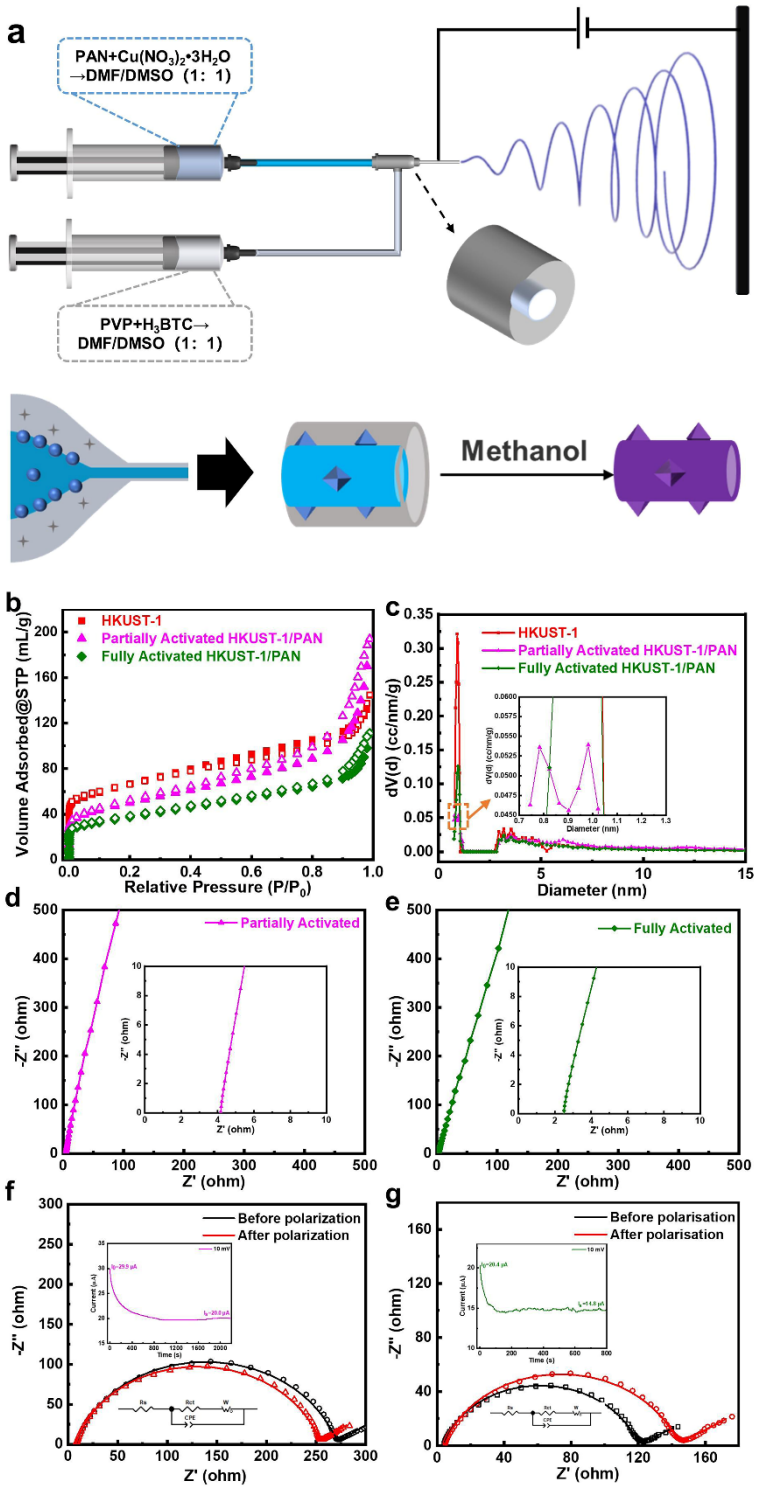

Fig. S6 (a) Schematic of preparing partially activated HKUST-1/PAN, BET (b) and pore size distributions (c) of HKUST-1/PAN with different activation levels, ionic conductivity of partially activated (d) and fully activated (e) prepared CSE, lithium-ion mobility of partially activated (f) and fully activated (g) prepared CSE(internally constant current polarization curves and equivalent circuit)

Fig. S 6a displays the schematic of preparing partially activated HKUST-1/PAN. The PVP shell layer was removed and the main body of the core layer of PAN fibers was retained by methanol soaking and solvent exchange, and the clogged PVP within the pores of the MOF crystals was also removed by the treatment, resulting in the partial activation of the MOF crystals. **Fig. S 6b** and **c** displays the BET curves and pore size distributions of HKUST-1/PAN with different activation levels. It can be seen that the adsorption capacity of partially activated HKUST-1/PAN is higher, but its pore size distribution is not concentrated in the 0.9 nm pores that can be loaded with Li-IL, and although the increased pore size of 0.75 nm is favourable for the increase of gas adsorption, it has no effect on the loading of Li-IL. **Fig. S 6d** and **e** displays the room temperature ionic conductivity ionic conductivity of CSE prepared with different levels of activation HKUST-1/PAN. The partially activated prepared CSE has a thickness of 150 um, an intrinsic impedance of 4.16 Ω, and an ionic conductivity of 1.79×10^{-3} S cm^{-1}, and the fully activated prepared CSE has a thickness of 120 um, an intrinsic impedance of 2.49 Ω, and an Ionic conductivity of 2.40×10^{-3} S cm^{-1}. **Fig. S 6f** and **g** shows the room temperature Li-ion mobility number of CSE prepared by HKUST-1/PAN with different levels of activation, with 0.31 for CSE prepared by partial activation and 0.698 for CSE prepared by full activation. All of which suggests that the ionic conductivity and lithium ion mobility number were higher for the high loading system.

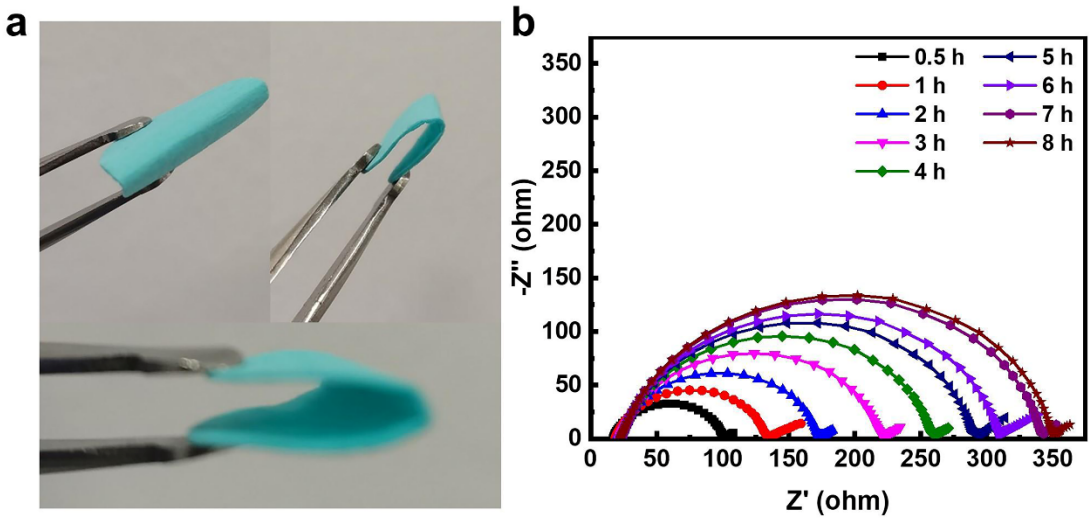

Fig. S7 Li-IL@HKUST-1/PAN SSE: a. flexibility, b. interface EIS varies with rest time

Fig. S 7a displays the Li-IL@HKUST-1/PAN CSE has good flexibility and can adapt to the volume change of the solid electrolyte/electrode interface. As shown in **Fig. S 7b**, the interfacial impedance diagram of the lithium symmetric battery assembled with this solid electrolyte changes over time. It can be seen that the interfacial impedance of Li-IL@HKUST-1/PAN solid electrolyte increases slowly within 0.5~8h, but becomes stable after 7h. It is indicated that Li-IL@HKUST-1/PAN solid electrolyte has good chemical stability for lithium metal.

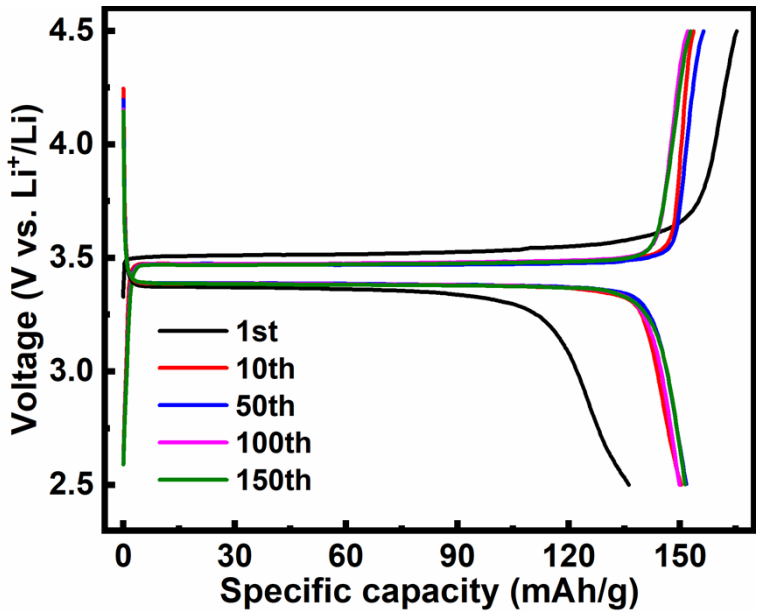

Fig. S8 Charge and discharge curve of different cycles at 0.1C

Fig. S8 displays the charge-discharge curves of the 1st, 10th, 50th ,100th and 150th cycles at 0.1C. Except for the 1st cycle due to the formation of SEI film by cell activation, the charge/discharge curves of the rest of the cycles are almost coincident, which proves that the performance of electrolyte is stable at this current density.

References

1 Q. Wang, T. Dong, Q. Zhou, Z. Cui, X. Shangguan, C. Lu, Z. Lv, K. Chen, L. Huang, H. Zhang and G. Cui, An in-situ generated composite solid-state electrolyte towards high-voltage lithium metal batteries, *Sci. China Chem.*, 2022, **65**, 934-942.

2 J. Zhang, N. Zhao, M. Zhang, Y. Li, P. K. Chu, X. Guo, Z. Di, X. Wang and H. Li, Fl exible and ion-conducting membrane electrolytes for solid-state lithium batteries: Dispersion of garnet nanoparticles in insulating polyethylene oxide, *Nano Energy*, 2016, **28**, 447-454.

3 H. Huo, Y. Chen, J. Luo, X. Yang, X. Guo and X. Sun, Rational Design of Hierarchical "Ceramic-in-Polymer" and "Polymer-in-Ceramic" Electrolytes for Dendrite-Free Solid-State Batteries, *Adv. Energy Mater.*, 2019, **9**, 1804004.

4 W. Li, S. Zhang, B. Wang, S. Gu, D. Xu, J. Wang, C. Chen and Z. Wen, Nanoporous Adsorption Effect on Alteration of the Li^+ Diffusion Pathway by a Highly Ordered Porous Electrolyte Additive for High-Rate All-Solid-State Lithium Metal Batteries, *ACS Appl. Mat er. Interfaces*, 2018, **10**, 23874-23882.

5 H. Wang, Q. Wang, X. Cao, Y. He, K. Wu, J. Yang, H. Zhou, W. Liu and X. Sun, Thi ol-Branched Solid Polymer Electrolyte Featuring High Strength, Toughness, and Lithium Io nic Conductivity for Lithium-Metal Batteries, *Adv. Mater.*, 2020, **32**, e2001259.

6 Z. Wang, S. Wang, A. Wang, X. Liu, J. Chen, Q. Zeng, L. Zhang, W. Liu and L. Zhan g, Covalently linked metal–organic framework (MOF)-polymer all-solid-state electrolyte me mbranes for room temperature high performance lithium batteries, *J. Mater. Chem. A*, 201 8, **6**, 17227-17234.

7 K. Pan, L. Zhang, W. Qian, X. Wu, K. Dong, H. Zhang and S. Zhang, A Flexible Cera mic/Polymer Hybrid Solid Electrolyte for Solid-State Lithium Metal Batteries, *Adv. Mater.*, 2020, **32**, e2000399.

8 H. Niu, N. Zhang, M. Ding, T. Hou, D. Zhang, L. Wang, P. Guan and X. Hu, Preparatio n of poly(ionic liquid) composite quasi-solid electrolyte by incorporating metal-organic fra mework filler decorated with ionic liquid for lithium batteries, *Solid State Ionics*, 2022, **38 0**, 115945.

9 Z. Wang, Z. Wang, L. Yang, H. Wang, Y. Song, L. Han, K. Yang, J. Hu, H. Chen and F. Pan, Boosting interfacial Li^+ transport with a MOF-based ionic conductor for solid-state batteries, *Nano Energy*, 2018, **49**, 580-587.

10 Z. Wang, R. Tan, H. Wang, L. Yang, J. Hu, H. Chen and F. Pan, A Metal-Organic-Fram ework-Based Electrolyte with Nanowetted Interfaces for High-Energy-Density Solid-State Li thium Battery, *Adv. Mater.*, 2018, **30**, 1704436.

11 Z. Wang, H. Zhou, C. Meng, W. Xiong, Y. Cai, P. Hu, H. Pang and A. Yuan, Enhancin g Ion Transport: Function of Ionic Liquid Decorated MOFs in Polymer Electrolytes for Al l-Solid-State Lithium Batteries, *ACS Appl. Energy Mater.*, 2020, **3**, 4265-4274.

12 M. Li, T. Chen, S. Song, Y. Li and J. Bae, HKUST-1@IL-Li Solid-state Electrolyte with 3D Ionic Channels and Enhanced Fast Li^+ Transport for Lithium Metal Batteries at High Temperature, *Nanomaterials*, 2021, **11**, 736.